Vibrational Mean Free Paths and Thermal Conductivity Accumulation Functions for Amorphous Materials

Jason M. Larkin[1] and Alan J. H. McGaughey[1]

[1]*Department of Mechanical Engineering*

Carnegie Mellon University

Pittsburgh, PA 15213

(Dated: July 26, 2013)

Abstract

Understanding thermal transport in crystalline systems requires detailed knowledge of phonons, which are the quanta of energy associated with atomic vibrations. By definition, phonons are non-localized vibrations that propagate energy over distances much larger than the atomic spacing. For disordered materials (e.g., alloys, amorphous phases), with the exception of very long-wavelength (low-frequency) modes, the vibrational modes are non-propagating. The film thickness and temperature dependence of thermal conductivity measured by experiments show (indirectly) that propagating modes contribute significantly to thermal conductivity for a-Si but not a-SiO2. Recent measurements by Regner et al. using a broadband FDTR technique argue that these propagating vibrational mean free paths can be probed to measure the thermal conductivity accumulation function for a-SiO2 and a-Si. Using lattice dynamics calculations and molecular dynamics simulations on realistic models of a-SiO2 and a-Si, we predict and characterize the contributions from propagating and non-propagating vibrations to thermal conductivity. The vibrational mean free paths are predicted for a-SiO2 and a-Si and the thermal conductivity accumulation function is compared with experimental broadband FDTR and varying thin film thicknesses measurements. For a-SiO2, the propagating modes are found to contribute negligibly for both bulk and thin film a-SiO2. We demonstrate using (to our knowledge) the largest model of bulk a-Si the scaling of the low frequency mode thermal diffusivities. Comparison of our model with the widely-varying experimental measurements show that the scaling of low-frequency mode diffusivities in a-Si thin films are well-described by our model of bulk a-Si *and* a scaling based on point defects. Further experiments are needed to understand how the low-frequency scaling of mode diffusivity varies with a-Si thin film thicknesses and preparation technique and suggestions are given based on the results from this work.

I. INTRODUCTION

Recently, experimental measurements of the thermal conductivity of amorphous materials such as amorphous silicon (a-Si)(cite) and amorphous SiN(cite) demonstrate that propagating (phonon-like) mode contribute significantly to thermal transport.(cite) However, the contribution of propagating modes to thermal transport in these amorphous materials is still not well understood. (cite) Traditionally, empirical expressions and simple models have been the only means to estimate MFPs in crystalline[1] and amorphous materials.(cite) Experimentally, inelastic neutron scattering has been used to measure phonon lifetimes in materials, but this technique is more suited for single crystal samples.[2] An x-ray diffraction and thermoreflectance technique can measure ballistic transport in some structures, but is not well-suited for amorphous thin films.[3] Koh et al. proposed a time-domain thermal reflectance (TDTR) technique with variation of modulation frequency to probe the low-frequency MFPs in crystals and alloys,[4] but this technique is limited by the modulation frequency and the theoretical understanding of the technique. (cite JAP paper) Studies have also been performed using frequency-domain thermal reflectance (FDTR) techniques to probe the accumulation function for bulk crystalline materials.[5,6] Broadband FDTR measurements by Regner argue that the thermal conductivity accumulation function for a-SiO2 and a-Si can be measured by varying the penetration depth of the experimental measurement.[7] However, understanding of the thermal conductivity accumulation function in amorphous materials is still not well understood.[8–13]

Recent broadband frequency domain thermal-reflectance experiments by Regner et al. measured how the thermal conductivity of a-SiO2 and a-Si thin films change with the penetration depth associated with the heating laser pulse.[7] For a-SiO2, the thermal conductivity of a 1000 nm film did not vary for penetration depths between 57 and 960 nm, suggesting that any propagating modes that contribute to thermal conductivity have MFPs below 57 nm. For a-Si, they find the thermal conductivities of thin films between 500 and 2000 nm vary by about 40% for penetration depths between 44 and 968 nm, suggesting that propagating modes with MFPs of 100 to 1000 nm contribute significantly to thermal conductivity.[7] Following the suggestion of Koh and Cahill, they interpret the measured value at a given penetration depth to be representative of the phonons with MFP less than that value, allowing for the construction of the so-called thermal conductivity accumulation function. Their

results are plotted in Fig. 8 for a 1000 nm thick film of a-SiO2 and in Fig. 7 for 500 nm (Regner A) and 2000 nm (Regner B) thick films for a-Si.[7]

Understanding the thermal conductivity accumulation function requires an understanding of the low-frequency propagating modes and the scaling of their MFPs with frequency.(cite) Experimental measurements of the thermal conductivity of thin films of a-SiO2 and a-Si at varying temperatures gives indirect information about the low-frequency propagating modes.(cite) For a-SiO2, varying temperature and film thickness[14,15] measurements all suggest that the propagating modes contribute a negligible amount to thermal conductivity. However, the behavior of the low-frequency modes has only recently been understood by experimental measurements.[16–20] For a-Si the low-frequency behavior of the MFPs is less understood. (cite) Temperature-varying(cite) and film thickness-varying measurements[8–12,21–28] suggest multiple different behavior of the low-frequency scaling of the mean free paths of vibrational modes in a-Si.

In this work, we perform Molecular Dynamics (MD) simulations and Lattice Dynamics calculations on large, realistic atomistic models of bulk a-SiO2 and a-Si. We predict the thermal conductivity of bulk a-Si using (to our knowledge) the largest MD simulation for a model of a-Si.(cite) The results are used to understand the recent experimental measurements of Regner et al. using broadband FDTR with varying penetration depths L_p.[7]

The spectrum of vibrational MFPs and the accumulated thermal conductivity are predicted for a-SiO2 and a-Si. Using a simple boundary scattering model, the accumulated thermal conductivities of a-SiO2 and a-Si thin films are predicted from our bulk models. Further experimentation is suggested based on the predictions from our models, previous experiments,[9,11,12,14,15,17,22,29–31] and emerging broadband thermoreflectance techniques.[4–7]

II. THEORETICAL FORMULATION

A. Vibrational Thermal Conductivity

We calculate the total vibrational thermal conductivity, k_{vib}, of an amorphous solids from

$$k_{vib} = k_{pr} + k_{AF}, \tag{1}$$

where k_{pr}[32–34] is the contribution from propagating (phonon-like) modes and k_{AF} is the contribution from diffusons (i.e., delocalized, non-propagating modes) predicted by the Allen-

Feldman (AF) theory.[8]

The propagating contribution is predicted from[8,10]

$$k_{pr} = \frac{1}{V}\int_0^{\omega_{cut}} DOS(\omega)C(\omega)D_{pr}(\omega)d\omega, \tag{2}$$

where V is the system volume, ω is the mode frequency, ω_{cut} is the maximum frequency of propagating modes, $DOS(\omega)$ is the vibrational density of states, $C(\omega)$ is the mode specific heat, and $D_{pr}(\omega)$ is the mode thermal diffusivity (see Eq. (4)).[8] The propagating contribution k_{pr} is written as an integral because the required use of finite simulation sizes[8,10] limit the lowest frequency modes that can be studied. An extrapolation must be made to the zero frequency limit.[8,9,12,17] Equation (2) is obtained using the single-mode relaxation time approximation to solve the Boltzmann transport equation for a phonon gas.[34]. In the derivation of Eq. (2), the system is assumed to be isotropic (which is valid for an amorphous material) and a single polarization,(cite) making the mode properties only a function of frequency. The choice of single phonon polarization (i.e., an averaging of the transverse and longitudinal branches) does not significantly change the results predicted in this work or that of others.[8–12,17] We write Eq. (2) in terms of the mode diffusivities to align with the diffuson theory,[8] which is described later in this Section.

We will evaluate Eq. (2) under the Debye approximation, which assumes isotropic and linear dispersion such that the the density of states is

$$DOS(\omega) = \frac{3\pi\omega^2}{2v_{s,DOS}^3}, \tag{3}$$

where v_s is an appropriate sound speed.[32] Since we use classical MD simulations,[35] we take the specific heat to be $C(\omega) = k_{\mathrm{B}}$ in the harmonic limit, where k_{B} is the Boltzmann constant. This harmonic approximation has been shown to be valid for a-Si modeled using the Stillinger-Weber potential at the temperatures of interest here (300 K) for low-frequency modes.[8] Taking the classical limit for the specific heat allows for a direct comparison between the MD- and lattice dynamics-based methods in our modeling framework.

The diffusivity of the propagating modes is

$$D_{pr}(\omega) = \frac{1}{3}v_s^2\tau(\omega), \tag{4}$$

where $\tau(\omega)$ is the mode lifetime.[34] An equivalent physical picture in terms of a scattering

length is

$$D(\omega) = \frac{1}{3} v_s \Lambda(\omega), \tag{5}$$

where $\Lambda(\omega)$ is the phonon mean free path (MFP), defined as

$$\Lambda(\omega) = v_s \tau(\omega). \tag{6}$$

The lifetimes will be modeled using

$$\tau(\omega) = B\omega^{-n}. \tag{7}$$

For amorphous materials, the scaling exponent n has been found experimentally and numerically to be between 2 and 4,[8,10–12,16,18–20,36–56] where $n = 2$ corresponds to Umklapp scattering[57] and $n = 4$ corresponds to Rayleigh scattering from point defects.[58] Combined with the form of the $DOS(\omega)$ [Eq. (3)] choosing $n \leq 2$ ensures that the thermal conductivity evaluated from Eq. (2) is finite. Choosing $n > 2$ causes the thermal conductivity to diverge, which can be fixed using additional anharmonic[8,10] or boundary scattering.[9,11,12]

The AF diffuson contribution to thermal conductivity is[8,10]

$$k_{AF} = \frac{1}{V} \sum_{\omega_i > \omega_{cut}} C_i(\omega) D_{AF,i}(\omega), \tag{8}$$

where ω_i is the frequency of the ith diffuson mode, $C_i(\omega_i)$ is the diffuson specific heat, and $D_{AF,i}$ is the diffuson diffusivity. Equation (8) is written as a sum because there are enough high-frequency diffuson in the finite-size systems studied here to ensure a converged value.[8,10] The AF diffusivities are predicted by[59]

$$D_{AF,i} = \frac{\pi V^2}{\hbar^2 \omega_i^2} \sum_{j \neq i} |S_{ij}|^2 \delta(\omega_i - \omega_j), \tag{9}$$

where $\hbar$ is Planck's constant and δ is the Dirac delta function. The heat current operator S_{ij}, which measures the thermal coupling between vibrational modes i and j based on their frequencies and spatial overlap of eigenvectors, can be calculated from harmonic lattice dynamics theory.[8,10,59] For Eq. (9), S_{ij} is directionally averaged because the amorphous materials studied in this work are isotropic. The diffuson specific heat is taken to be k_{B} to allow for the comparison between the MD- and LD-based methods.

The form of Eq. (1) has been used in several previous studies of amorphous materials with varying assumptions.[8–12,17,17,55] The various assumptions all lead to predictions that

k_{pr} is a negligible ($< 10\%$) and non-negligible ($> 20\%$) fraction of k_{vib} for a-SiO2[17] and a-Si[8–12,55], respectively.

(NOT HERE) While predictions for the contributions to the total vibrational thermal conductivity k_{vib} from propagating (k_{pr}) and non-propagating (k_{AF}) have been made for a-SiO2 and a-Si,(cite) no thermal conductivity accumulation functions have been predicted to compare with Regner. (cite) Using lattice dynamics calculations and molecular dynamics simulations of large-scale (4000 atom models), we predict the inputs to Eq. (1) in Sections IV A, IV B, IV E, and the bulk thermal conductivity k_{vib} and its contributions k_{pr} and k_{AF} in Section V A Using very large-scale (up to $800,000$ atoms) MD simulations, we predict the thermal thermal conductivity k_{vib} of bulk a-SiO2 and a-Si to compare with the predictions based on the mode-by-mode properties. For the first time, the MFPs of propagating modes in bulk a-SiO2 and a-Si are used with a boundary scattering model to predict the thermal conductivity accumulation, which is compared with experimental thin film measurements and broadband FDTR measurements of a-SiO2 and a-Si in Section V B.

B. Thermal Conductivity and Diffusivity Limits

To interpret the non-propagating contribution k_{AF}, it is useful to consider a high-scatter (HS) limit for the mode diffusivity,

$$D_{HS} = \frac{1}{3} v_s a, \tag{10}$$

where it is assumed that all vibrational modes travel with the sound speed v_s and scatter over a distance of the lattice constant a.[30] Equation (10) leads to a high-scatter (HS) limit of thermal conductivity in the classical limit given by[30]

$$k_{HS} = \frac{k_{\mathrm{B}}}{V_b} b v_s a, \tag{11}$$

where V_b is the volume of the unit cell and b is the number of atoms in the unit cell. Equation (11) has been found to be a good lower limit for the thermal conductivity of a-SiO2[17,29,30], a-Si,[8–10,55], and other glasses.[22,60–63]

Kittel suggested that the thermal conductivity of glasses in the high-temperature limit could be interpreted using a temperature-independent high-scatter diffusivity similar to Eq. (10).[60] Kittel's theory implies that the modes that dominate thermal transport in glasses are

vibrations with MFPs $\Lambda = a$, such that $k_{vib} \approx k_{HS}$.[60,64] For models of amorphous Lennard-Jones argon[63] and a-GeTe[62], k_{vib} is predicted to be equal to k_{HS} within the errors. For a-SiO_2, $k_{vib} \approx 2k_{HS}$, but it is unclear what the appropriate lattice constant should be, making a factor of two reasonable. For a-Si, the experimentally measured thermal conductivity at a temperature of 300 K is $(1-6)k_{HS}$,[8–12,55] indicating that there may be a large contribution from k_{pr}.

(NOT HERE) We investigate the contributions k_{pr} and k_{AF} using detailed atomistic models for a-SiO2 and a-Si which are described in the next section.

III. CALCULATION DETAILS

A. Sample Preparation

The three smallest a-SiO_2 samples are the same as those used in Ref. 65 and contain 288 , 576, and 972 atoms. These samples were originally prepared using a melt-quench procedure. Using the same procedure, larger systems of N_a = 2880, 4608, and 34,562 were created by tiling the smaller samples. The entire melt-quench procedure was performed at constant volume.[65] The tiled samples were first melted at a temperature of 10,000 K in a cubic simulation cell. The liquid was then quenched instantaneously to 300 K and annealed for 10 ns.

The largest sample has 34,562 atoms and a supercell side length of 8.052 nm. All samples were simulated at a density, ρ, of 2350 kg/m^3.[65] The atomic interactions are modeled using a modified BKS potential from Ref. 65, except that the 24-6 Lennard-Jones (LJ) potential is changed to a 12-6, which has a negligible effect on the predictions. The LJ potentials use a cutoff of 8.5 $\mathring{A}$ and the Buckingham potential uses a cutoff of 10 $\mathring{A}$. The electrostatic interactions are handled using the Wolf direct summation method with exponential parameter $\eta = 0.223\mathring{A}^{-1}$ and a cutoff of 12 $\mathring{A}$.[66]

For a-Si, we use models generated using the modified Wooten-Winer-Weaire (WWW) algorithm from Ref. 67. Sample sizes with 216, 1000, 4096, and 100,000 atoms. Similarly-large models of a-Si were studied in Ref. 55 using the MD-based direct method to predict thermal conductivity. A large sample was created from the 100,000 atom sample by treating it as a unit cell and tiling twice in all directions to create an 800,000 atom sample with

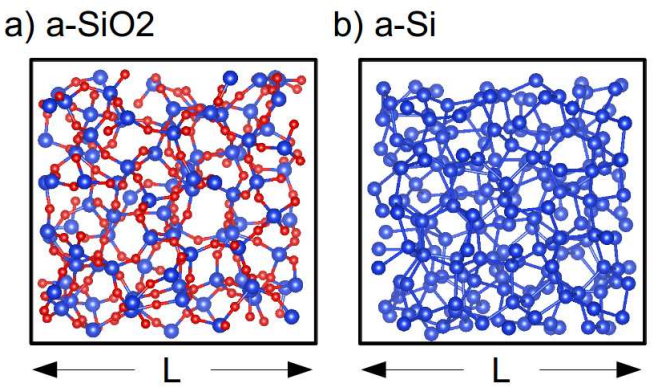

FIG. 1: (a) a sample supercell of a-SiO2 with 288 atoms and supercell side length 1.597 nm. Samples up to $4,608(36,864)$ atoms and side length $L4.026(8.052)$ nm are used for the LD(MD)-based methods in Sections IV D and IV E. The samples were prepared using a melt-quench technique (see Section III A). (b) a sample supercell of a-Si with 216 atoms and side length 1.086 nm. Samples up to size $4,096(800,000)$ atoms and side length 4.344(24.81) nm are used for the LD(MD)-based methods in Sections IV D and IV E. The a-Si samples were prepared using a modified WWW algorithm (see Section III A). Both a-SiO2 and a-Si structures are visualized using the VESTA package.[71]

supercell side length of 24.81 nm. All a-Si structures have a density of 2330 kg/m^3, equivalent to the perfect crystal with a lattice constant of 5.43 $\mathring{A}$. The Stillinger-Weber potential models the atomic interactions.[68]

Amorphous materials may have many different atomic configurations with nearly equivalent potential energies leading to potential metastability during MD simulations.[10,55,69,70] This meta-stability can cause errors when predicting vibrational lifetimes using Normal Mode Decomposition (NMD, see Section IV D).(cite) To remove metastability, all Both a-SiO2 and a-Si samples were annealed at a temperature of 1100 K for 10 ns.[10,55] The removal of meta-stability is demonstrated by a decrease and plateau of the sample's potential energy. Small samples of a-SiO2 and a-Si are shown in Fig. 1.

B. Simulation Details

Molecular dynamics (MD) simulations are performed using the a-SiO_2 and a-Si supercells described in Section III A. The MD simulations were performed using LAMMPS[72] with

time steps of dt = 0.905(0.5) fs for a-SiO_2(a-Si). Ten MD simulations with different initial conditions were run and the predictions from these simulations were ensemble averaged. All MD simulations are first equilibrated in an NVT (constant number of atoms, volume, and temperature) ensemble for 10^6 time steps. Data are then collected from simulations in the NVE (constant number of atoms, volume, and total energy) ensemble for 2^{21} time steps where the atomic trajectories are sampled every 2^8 time steps.

The Green-Kubo (GK) method is used to predict a top-down thermal conductivity k_{GK} (i.e., without using Eq. (1)). The k_{GK} is predicted by window averaging the integral of The first-avalanche method is used to predict k_{GK}.[73] For system sizes of 4,608(4,096) atoms, the trajectories from the MD simulations used for the GK prediction method are also used with the NMD method to predict the vibrational mode lifetimes for a-SiO2(a-Si) for use in Eq. (1) (Section IV D).

For the amorphous supercells studied, the only allowed wave vector is the gamma-point (i.e., $\boldsymbol{\kappa} = 0$), where $\boldsymbol{\kappa}$ is the wavevector and there are $3N_a$ polarization branches labeled by ν. Calculation of the vibrational modes at the Gamma point requires the eigenvalue solution of a dynamical matrix of size $(3N_a)^2$ that scales as $[(3N_a)^2]^3$, limiting the system sizes that can be considered to 4,608(4,096) atoms for a-SiO_2(a-Si). The eigenvalue solution is required to predict the vibrational DOS (Section IV A) and structure factors (Section IV B), and to perform the NMD technique (see Section IV D) and AF calculations (see Section IV E). The frequencies and eigenvectors were computed using harmonic lattice dynamics calculations and GULP.[74] The calculation of the AF thermal diffusivities [Eq. (9)] is performed using GULP and a Lorentzian broadening of $14\delta\omega_{avg}(5\delta\omega_{avg})$ for a-SiO_2(a-Si), where $\delta\omega_{avg}$ is the average mode frequency spacing [$\delta\omega_{avg} =$ () for a-SiO2(a-Si)].[8,10] For a-Si the broadening used here is within 20% of that used in Ref 10. Varying the broadening around these values does not change the resulting thermal conductivity k_{AF} significantly (see Section V A).

IV. VIBRATIONAL PROPERTIES

A. Density of States

In this section, we examine the vibrational frequencies and DOS for a-SiO_2 and a-Si. The vibrational DOS is computed from

$$DOS(\omega) = \sum_i \delta(\omega_i - \omega), \tag{12}$$

where a unit step function of width $100\delta\omega_{avg}$ is used to broaden $\delta(\omega_i - \omega)$. Results are plotted in Fig. 2 using a broadening of $10\delta\omega_{avg}$ and . Because of the finite model size, the low-frequency modes are sparse and the DOS can depend on the broadening. This broadening is large enough to obtain a smooth DOS but small enough to capture the low frequency behavior.[10]

The DOS for a-Si is similar to the DOS of crystalline silicon,[75,76] with pronounced features at mid- and high-frequencies. The DOS for a-SiO_2 is constant over most of the frequency-range, with a gap at the higher frequencies that separates the Si-O interactions.[65] There is a clear ω^{-2} scaling for both a-Si and a-SiO_2 at the lowest frequencies. The onset of this scaling occurs at a higher frequency for a-Si than a-SiO_2. This low-frequency scaling is predicted by the Debye model [Eq. (3)] and suggests that these modes may be propagating (i.e., phonon-like).

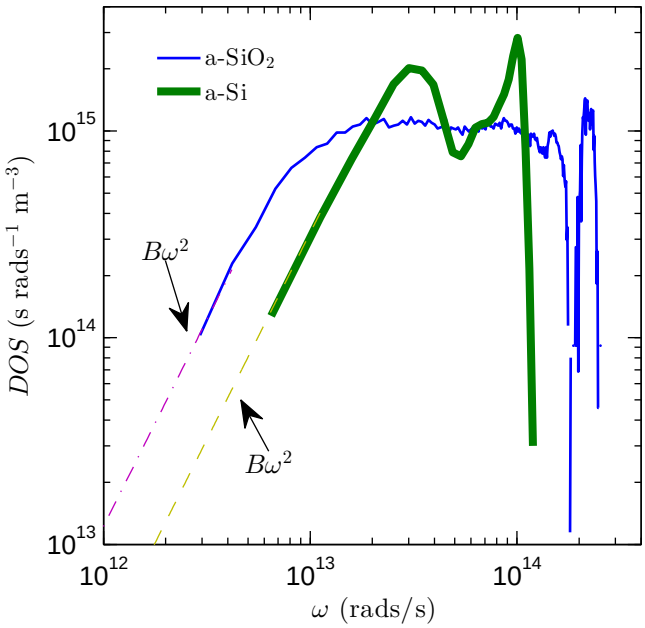

FIG. 2: Vibrational DOS predicted for a-SiO2 and a-Si. Both models show an ω^{-2} scaling at low frequency.

B. Structure Factor

Calculating the structure factors of the supercell Gamma modes is a method to test for their propagating (plane-wave) character at a particular wave vector and polarization and has been previously used to predict effective dispersion curves of amorphous materials experimentally[77,78](more) and numerically.[8,10,39–41,44,46,49,54,63,79–85] The structure factor at a wave vector $\boldsymbol{\kappa}$ is defined as[80]

$$S^{L,T}(\substack{\boldsymbol{\kappa}\\ \omega}) = \sum_{\nu} E^{L,T}(\substack{\boldsymbol{\kappa}\\ \nu})\, \delta(\omega - \omega(\substack{\boldsymbol{\kappa}=\mathbf{0}\\ \nu})), \tag{13}$$

where the summation is over the Gamma modes, E^T refers to the transverse polarization and is defined as

$$E^{L}(\substack{\boldsymbol{\kappa}\\ \nu}) = \left| \sum_{b} \hat{\boldsymbol{\kappa}} \cdot e(\substack{\boldsymbol{\kappa}=\mathbf{0}\ b\\ \nu\ \ \alpha}) \exp[i\boldsymbol{\kappa} \cdot \boldsymbol{r}_0(\substack{l=0\\ b})] \right|^2 \tag{14}$$

and E^L refers to the longitudinal polarization and is defined as

$$E^{T}(\substack{\boldsymbol{\kappa}\\ \nu}) = \left| \sum_{b} \hat{\boldsymbol{\kappa}} \times e(\substack{\boldsymbol{\kappa}=\mathbf{0}\ b\\ \nu\ \ \alpha}) \exp[i\boldsymbol{\kappa} \cdot \boldsymbol{r}_0(\substack{l=0\\ b})] \right|^2 . \tag{15}$$

In Eqs. (14) and (15), the b summations are over the atoms in the disordered supercell, $\boldsymbol{r}_0(\substack{l=0\\ b})$ refers to the equilibrium atomic position of atom b, l labels the unit cells ($l = 0$ for the supercell), α labels the Cartesian coordinates, and $\hat{\boldsymbol{\kappa}}$ is a unit vector. The vibrational mode shape is contained in the $3N_a$ components of its eigenvector, $e(\substack{\boldsymbol{\kappa}=\mathbf{0}\ b\\ \nu\ \ \alpha})$.(cite)

The transverse and longitudinal structure factors $S^{L,T}(\substack{\boldsymbol{\kappa}\\ \omega})$ are plotted in Figs. 3(a) and 3(b) for a-SiO_2 and a-Si for wavevectors along the [100] direction of the supercells. Because amorphous structures are isotropic, the structure factors are direction-independent. The wavenumbers are normalized by $2\pi/a$, where a is 4.8(5.43) $\mathring{A}$ for a-SiO_2(a-Si), which is based on the lattice constants of c-SiO2(c-Si).[65,68]

Mode frequencies [$\omega_0(\kappa)$] and linewidths [$\Gamma(\kappa)$] can be predicted by fitting each structure factor peak $S^{L,T}(\substack{\boldsymbol{\kappa}\\ \omega})$ to a Lorentzian function

$$S^{L,T}(\substack{\boldsymbol{\kappa}\\ \omega}) = \frac{C_0(\boldsymbol{\kappa})}{[\omega_0(\boldsymbol{\kappa}) - \omega]^2 + \Gamma^2(\boldsymbol{\kappa})}, \tag{16}$$

where $C_0(\nu)$ is a constant related to the DOS.[84] A dispersion relation is identified by plotting $\omega_0(\kappa)$ values in the middle panels of Figs. 3(a) and 3(b), where the error bars indicate the linewidths.

For a-Si, the peaks are reasonably Lorentzian for all wavenumbers.[46] For a-SiO2, the peaks are well-approximated as Lorentzian only at the smallest wavenumbers. For large wavenumber, the structure factors peaks are less than an order of magnitude larger than the background, and the widths are on the order of the total frequency range.

For a-Si, the extracted dispersion is nearly linear at small wavenumbers with a slight decrease in slope at the largest values.[8,10] For a-SiO2, the dispersion is concave-down for the smallest wavenumbers considered, transitioning to a strong concave-up dispersion at intermediate wavenumbers. For the intermediate wavenumbers, the longitudinal dispersion for a-SiO_2 is well-described by the so-called "dispersion law for diffusons", where $\omega \propto \kappa^2$.[84] This large concave-up dispersion has been observed in various amorphous models[17,46,86] including a-SiO2.[17,86] We note that at frequencies lower than 100 GHz, experimental measurements of a-SiO2 recover a linear dispersion.[17,18,20]

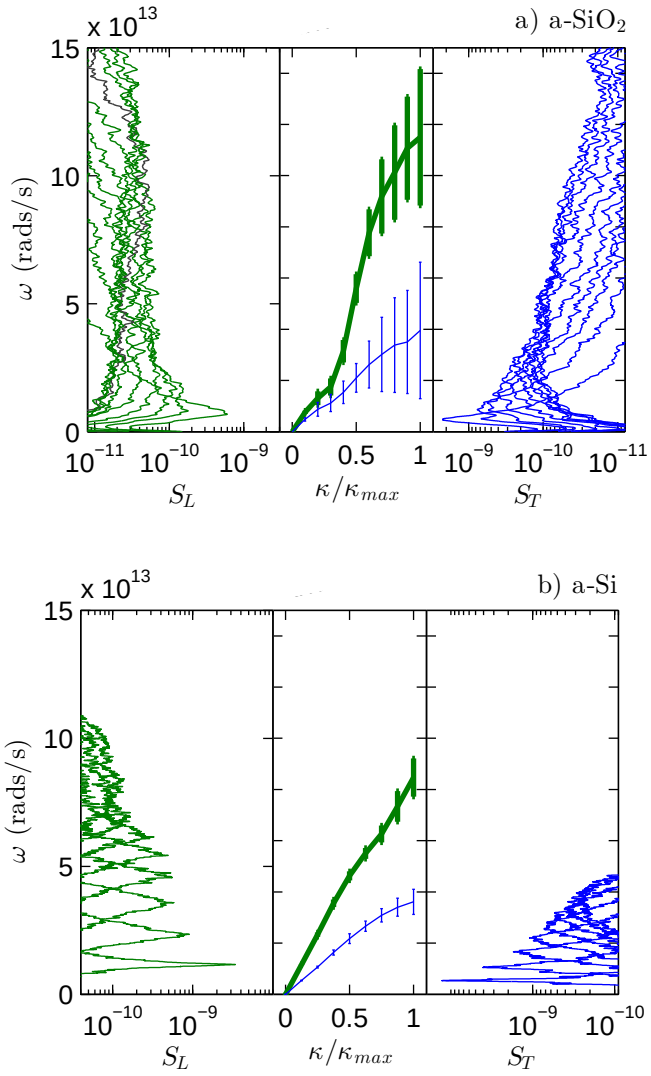

FIG. 3: Longitudinal (left panel) and transverse (right panel) structure factors (Eq. (13)) for a-SiO2 (top plot) and a-Si (bottom plot). Sound speeds are estimated by finite differencing (Eq. (17)) of the lowest frequency peaks and are reported in Table I. The dispersion for a-SiO2 is only non-linear for all wavenumbers. The dispersion for a-Si is nearly-linear over a wide range of wavenumber. Lifetimes are predicted from the widths of the structure factor peaks (Eq. (16)) and are plotted in Fig. 4.

C. Group Velocity

For a disordered solid, except for the transverse and longitudinal sound speeds, there is not an accepted method to predict the group velocity of each vibrational mode. While the structure factor gives the frequency spectrum needed to construct a propagating state with pure wavevector $\boldsymbol{\kappa}$, the mode spectra $E^T(\overset{\boldsymbol{\kappa}}{\nu})$ and $E^L(\overset{\boldsymbol{\kappa}}{\nu})$ predict the plane-wave character of each mode. It is not generally possible to assign a unique wavevector to individual modes, even at low frequency,[8,79,87] which makes predicting individual mode group velocities challenging. Attempts have been made to predict individual mode group velocities,[13,55,76,88,89] but there is no theoretical basis for these methods.

We now use the DOS and structure factors predicted in Sections IV A and IV B to predict the group velocity of the low-frequency modes for a-SiO2 and a-Si. By fitting the DOS from Fig. 2 to Eq. (3), a sound speed $v_{s,DOS}$ is obtained and is reported in Table I. Because the DOS is a mixture of transverse and longitudinal modes, only a single sound speed can be predicted. Both longitudinal and transverse sound speeds can be predicted from the structure factor peaks by finite differencing the equation

$$v_s = \frac{\delta\omega_0(\kappa)}{\delta\kappa}. \tag{17}$$

The results for the lowest frequencis are provided in Table I. The transverse and longitudinal sound speeds of a material can also be predicted from the material's bulk (G) and shear (K) moduli from

$$v_{s,T} = \frac{G}{\rho}^{1/2}, \tag{18}$$

and

$$v_{s,L} = \frac{4G + 3K}{3\rho}^{1/2}. \tag{19}$$

We use the bulk and shear moduli defined in terms of the elastic constants according to the Voight convention.[74] The corresponding sound speeds are reported in Table I. The longitudinal and transverse sound speeds predicted for a-Si are in good agreement with those found in a previous study using a similar model.[8,10] Comment about a-SiO2 sound speeds with expt and modeling.(cite)

By comparing the sound speeds in Table I, it is clear that the DOS of our models for a-Si and a-SiO_2 are characterized by using the transverse sound speeds. The transverse sound speeds obtained from the elastic moduli are larger than those from the structure factors,

TABLE I: Longitudinal and transverse sound speed estimated from the elastic constants [Eqs. (19) and (18)], DOS (3), and structrue factors (Eq. (17)). The pre-annealed group velocities predicted by the elastic constants are $v_{s,T} = 3,670$, $v_{s,L} = 7,840$ for a-Si and $v_{s,T} = 2,541$, $v_{s,L} = 4,761$ for a-SiO2 (see Section IV B).

method	Eqs. (18), (19)	Eqs. (13), (17)	DOS Eq. (3)
a-SiO_2			
transverse	3,161	2,732	2,528
longitudinal	5,100	4,779	
a-Si			
transverse	3,886	3,699	3,615
longitudinal	8,271	8,047	

which results from the concave-down dispersion seen at low κ, particularly for a-SiO2 (Fig.).(cite) For a-SiO2, the concave-down dispersion also affects the low-frequency DOS, where the predicted sound speed $v_{s,DOS}$ is less than that predicted from the structure factor and the elastic constants. The concave-down dispersion is less pronounced for a-Si, where the sound speeds predicted by all three methods are within five percent of each other.

Under the Debye model (Eq. (3)), the *smaller* transverse sound speed makes the *larger* contribution to the DOS which scales as the sound speed cubed. For a-Si and a-SiO2 the contribution from longitudinal modes to the Debye DOS is nearly an order of magnitude less than the transverse modes for a given frequency interval. For a-SiO_2, the longitudinal and transverse sound speeds are closer, but the non-linear dispersion is stronger than a-Si (Fig. 3).(cite) The intensity of the structure factors, which are directly proportional to the DOS,[84] for transverse polaritzations was found to be four to five[90] and six to eight[44] times larger than longitudinal polarizations for models of a-SiO2, which supports our finding that the DOS is dominated by transverse modes. The transverse sound speed predicted by the DOS, $v_{s,DOS}$, is used for both a-SiO_2 and a-Si throughout the rest of this work and is discussed in Section V A.

D. Lifetimes

We now predict the lifetimes of all vibrational modes in our models of a-SiO2 and a-Si using the MD simulation-based NMD method.[55,89,91–95] The NMD-predicted lifetimes will be compared with the timescales extracted from the structure factor linewidths, $\tau_{SF} = 1/2\Gamma(\kappa)$ (Section IV B, (Eq. (16))). The NMD method explicitly includes the disorder in the supercell.[13,55,63,96,97]

In NMD, the atomic trajectories from MD simulations are first mapped onto the vibrational mode coordinate time derivative,[33]

$$\dot{q}(\substack{\boldsymbol{\kappa}=\mathbf{0}\\ \nu};t) = \sum_{\alpha,b,l}^{3,n,N} \sqrt{\frac{m_b}{N}} \dot{u}_\alpha(\substack{l\\ b};t)\, e^*(\substack{\boldsymbol{\kappa}=\mathbf{0}\ b\\ \nu\ \ \alpha}) \exp[i(\mathbf{0}\cdot\mathbf{r}_0(\substack{l\\ 0}))]. \tag{20}$$

Here, m_b is the mass of the b_{th} atom in the supercell, u_α is the α-component of the atomic displacement from equilibrium, $\dot{u}_\alpha$ is the α-component of the atomic velocity, and t is time. Because the supercells of a-SiO2 and a-Si are disordered, the NMD method is performed at the wavevector $\boldsymbol{\kappa} = \mathbf{0}$. The spectral energy of each vibrational mode, $\Phi(\substack{\boldsymbol{\kappa}\\ \nu};t)$, is calculated from

$$\Phi(\nu,\omega) = \lim_{\tau_0\to\infty} \frac{1}{2\tau_0} \left| \frac{1}{\sqrt{2\pi}} \int_0^{\tau_0} \dot{q}(\substack{\boldsymbol{\kappa}=\mathbf{0}\\ \nu};t) \exp(-i\omega t) dt \right|^2. \tag{21}$$

We choose the frequency domain representation of the normal mode energy because it is less sensitive to metastability of the amorphous structure.

The vibrational mode frequency and lifetime are predicted by fitting each mode's spectral energy $\Phi(\nu,\omega)$ to a Lorentzian function,

$$\Phi(\nu,\omega) = \frac{C_0(\nu)}{[\omega_0(\nu)-\omega]^2 + \Gamma^2(\nu)}, \tag{22}$$

where the constant $C_0(\nu)$ is related to the average mode energy of each mode and the linewidth $\Gamma(\nu)$ and is valid when $\Gamma(\nu) << \omega_0(\nu)$.[95] The mode lifetime is[91,94]

$$\tau(\nu) = \frac{1}{2\Gamma(\nu)}. \tag{23}$$

The NMD-predicted lifetimes are plotted in Fig. 4 for a-SiO2 and a-Si. For a-SiO2, the mode lifetimes are generally larger than the Ioffe-Regel (IR) limit $\tau = 2\pi/\omega$,[39] and follow this limit at low frequency. There is no clear evidence for an ω^{-2} scaling, which corresponds

to propagating modes. At mid frequencies the mode lifetimes are constant. There is a peak near 2 $\times 10^{14}$ rads/s which corresponds to a peak in the DOS (see Fig. 2). The lifetimes predicted from the structure factor fall below the NMD-predicted lifetimes and the IR limit. These low values result because the structure factor for a-SiO2 is evaluated for wavenumbers where the peaks are not well-approximated as Lorentzian. (cite) Furthermore, the linewidths (the inverse of the lifetime) are on the order of the frequencies. Previous modeling and theoretical predictions show that the structure factor begins to take on the form of the DOS for large enough wavenumber,[17,82] and that the linewidths (timescales) are not meaningful.

For a-Si, the mode lifetimes show a clear ω^{-2} scaling at low frequency. The lifetimes plateau at higher frequencies, over a wider range of frequencies than a-SiO2, with two peaks corresponding to peaks in the DOS (Fig. 2). A similar plateau of lifetimes at high frequencies has been reported for disordered lattices[63,98] and other models of a-Si.[55] The transition from the low-frequency scaling to the plateau region occurs near 10^{14} rads/s, which corresponds to where the DOS peaks in Fig. 2. Similar behavior has been observed for models of disordered lattices.[63] The lifetimes predicted by the structure factor are in good agreement with those predicted by NMD at low frequencies. Similar agreement has been reported in other models of amorphous materials.[99]

The NMD-predicted lifetimes in this work are similar in magnitude to those predicted for previous models of a-Si.[100–103] Fabian and Allen find lifetimes on the order of picoseconds for a-Si[101] and para-crystalline silicon.[103] A previous study of a-Si modeled using the Tersoff potential predicted vibrational lifetimes on the order of 100 ps, an order of magnitude larger than the values reported here and in previous studies.[100–103] It is unclear what the source of this discrepancy is, although in Ref 13 the NMD analysis was performed in the time domain where metastability can be more strongly pronounced. Using the Tersoff potential on the WWW a-Si models in this work we predict similar lifetimes to the SW potential. Predicted lifetimes are also similar for samples created using a melt-quench technique (see Section III A).

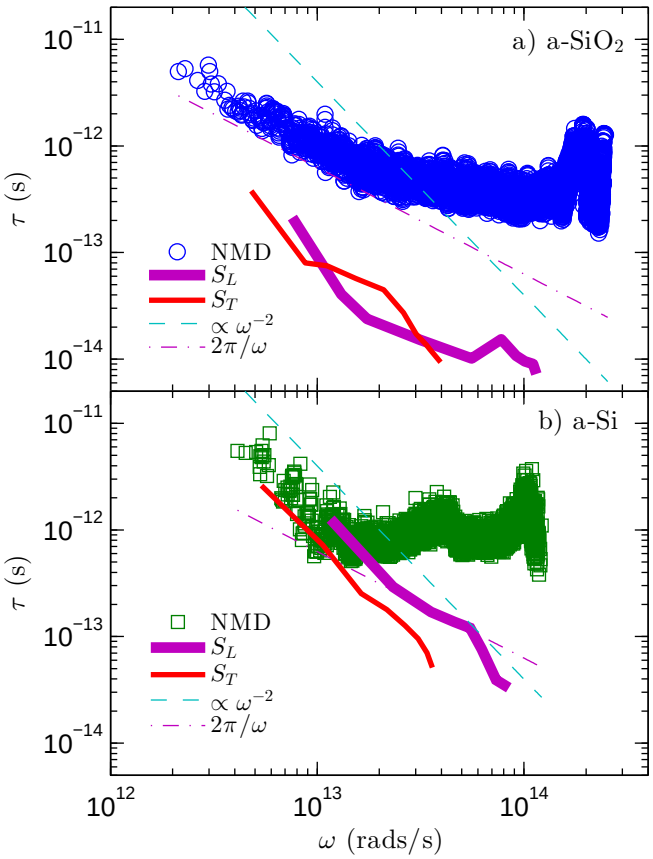

FIG. 4: Vibrational mode lifetimes predicted by NMD [Eq. (23)] and the structure factors [Eq. (16)] for (a) a-SiO2 and (b) a-Si. The NMD-predicted lifetimes are larger than the IR limit while the lifetimes predicted from the structure factors fall below this limit, particularly for a-SiO2. The NMD-predicted lifetimes show a plateau at high-frequencies For both systems, while a clear ω^{-2} scaling is observed for a-Si.

E. Diffusivities

Using the sound speeds predicted from the DOS $v_{s,DOS}$ (Table I), the NMD-predicted lifetimes for a-SiO2 and a-Si are used to predict the mode diffusivities with Eq. (4) and are plotted in Fig. 5. We note that the sound speed is most appropriate for the lowest-frequency modes where the DOS scales as ω^2 (Fig. 2). To compare with the NMD predictions, the AF theory is also used to predict the mode diffusivities which are also plotted in Fig. 5.

For a-SiO2, the mode diffusivities predicted by NMD and AF agree well over the majority of the frequency range. At high frequencies the diffusivities do not vary much, except for a

peak for the NMD predictions near 2 $\times 10^{14}$ rads/s which corresponds to the same peak in lifetimes (Fig.). For the AF predictions, the mode diffusivities near 2 10^{14} rads/s and at the highest frequencies show a sharp decrease, which is an indication that these modes are localized.[8] In the mid-frequency range, the mode diffusivities are larger than the high-scatter limit [Eq. (10)].

For a-SiO2 at the lowest frequencies, the diffusivities scale roughly as ω^{-2}. This scaling is not definitive, however, for the diffusivities predicted by either method, particularly for the NMD predictions. Because there is no clear transition from propagating to non-propagating modes, we choose $\omega_{cut} = 4.55 \times 10^{12}$ rad/s for Eq. (1) based on Ref 17 where the lowest frequency was limited by the experimental technique. This choice is discussed in Section V A. The constant B in Eq. (7) is fit to the AF-predicted diffusivities for $\omega \leq \omega_{cut}$.

For a-Si the mode diffusivities predicted by NMD and AF low frequencies show a clear ω^{-2} scaling. The NMD-predicted diffusivities are larger and show less scatter than those predicted by the AF theory, which is due to the finite-size system and the broadening which is required to evaluate Eq. (9).[8] By using a larger broadening ($100\delta\omega_{avg}$) the scatter in the AF-predicted diffusivities at low frequency can be smoothed, but at the cost of decreasing the diffusivities at intermediate and high frequencies which affects the predicted diffuson contribution to thermal conductivity kAF (see Section V A). It is possible that a frequency-dependent broadening may be necessary for a-Si and the AF theory, but determining this dependence is not necessary for interpreting our results. The NMD- and AF-predicted diffusivities diverge near 10^{13} rads/s indicating that the sound speed is no longer applicable. The diffusivities are larger than the high-scatter limit [Eq. (10)] except for the highest frequencies which are localized.[8]

For a-Si, we choose ω_{cut} and B so that Eq. (4) is equal to the AF-predicted diffusivity at $\omega = \omega_{cut}$. The resulting values are $\omega_{cut} = 1.1610^{1}3$ rads/s and $B = 2.76 \times 10^{14}$ s^{-1}. This choice allows Eq. (4) to pass reasonably well through both the AF and NMD-predicted diffusivities. For a-Si, we also consider a separate scaling for Eq. (7) with $n = 4$ that is discussed in Section V A. Because this scaling is not clear from the data in Fig. 5 we use $\omega_{cut} = 1.52 \times 10^{13}$ rads/s from Refs.[8] and[9] and choose B so that Eq. (4) is equal to the AF-predicted diffusivity at ω_{cut}. We discuss these choices in Section V A.

Both a-SiO_2 and a-Si have a region at higher frequencies where the AF-predicted mode diffusivities are relatively constant. This behavior has been reported for a number of

model disordered systems such as disordered lattices[63,84,98], amorphous solids,[13] and jammed systems.[51,53] For a-Si the NMD- and AF-predicted diffusivities diverge near 10^{13} rads/s, while the NMD-predicted lifetimes are relatively constant above this frequency.

While diffusons are non-propagating modes whose MFPs are not well-defined, a diffuson length scale can be defined as

$$\Lambda_{AF,i}(\omega) = [3D_{AF,i}(\omega)\tau_i(\omega)]^{1/2}, \tag{24}$$

where $\tau_i(\omega)$ are the NMD-predicted lifetimes. Using this definition, $\Lambda_{AF,i}(\omega)$ is found to vary for both a-SiO2 and a-Si between the supercell size and the lattice constant for modes with $\omega > \omega_{cut}$. Similar MFPs have been estimated for diffusons in a-Si in previous studies.[8,10] This result is in contrast to the MFPs estimated in Ref 55 which were found to be nearly two orders of magnitude larger than the system size. We believe that the origin of these large MFPs is a combination of the predicted lifetimes (see Section IV D) and the method used to estimate the mode group velocities.[55]

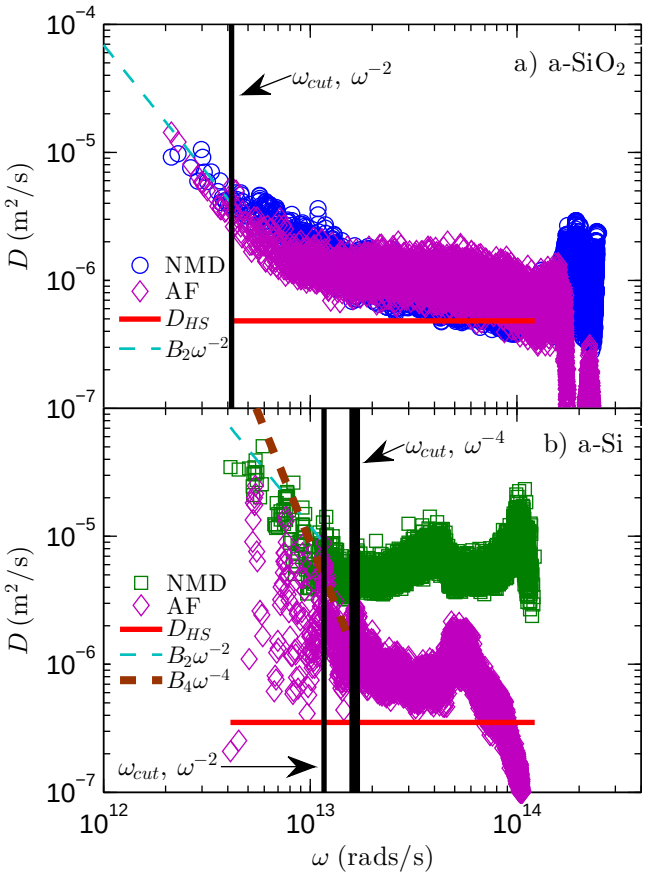

FIG. 5: Vibrational mode diffusivities predicted from NMD (using Eqs. (4) and (23)) with the sound speed $v_{s,DOS}$ from Table I) and the AF theory [Eq. (9)]. Also shown are extrapolations based on ω^{-2} and ω^{-4} scalings with Eqs. (7) and (4) for a-Si. For both systems the diffusivities are larger than the high-scatter limit [Eq. (10)] except at high frequencies where the modes are localized.[8]

V. THERMAL CONDUCTIVITY

A. Bulk

To predict the bulk thermal conductivity for our models of a-SiO2 and a-Si, we use Eq. (1) and the GK method. The GK method is computationally inexpensive compared to the NMD and AF methods so that larger system sizes can be studied (see Section III A). The GK-predicted thermal conductivities for a-SiO2 and a-Si are plotted in Fig. 6 for varying system sizes. For a-SiO2, there is no system-size dependence, and the bulk thermal conductivity is estimated to be 2.10 ± 0.20 W/m-K by averaging over all the predicted k_{GK}. This value is larger than experimental measurements, which range between 1.3[14,30] and 1.5 W/m-K,[7,15] because of the classical nature of the MD simulation (see Section II A). Quantum statistical effects are considered later in this section.

For a-Si, there is a clear system-size dependence. Because the low-frequency DOS has the form of Eq. (3) and the diffusivities scale as ω^{-2} the thermal conductivity will scale as the inverse of the system size. The bulk value can be found by extrapolating in an infinte system size.[95,104,105] The extrapolation is performed using the three largest system sizes, including the tiled 800,000 atom sample. We do not observe that tiling an a-Si model increases the thermal conductivity above the expected linear scaling as was found in Ref. 13 using the MD-based direct method. This finding is likely due to the small model used to perform the tiling in that study (512 atoms), while we use a large model (100,000 atoms). The extrapolated bulk value is 1.97 ± 0.15 W/m-K.

To predict thermal conductivity from Eq. (1) we use the parameters B and ω_{cut} specified in Section IV E assuming an ω^{-2} scaling below ω_{cut}, and the AF-predicted diffusivities obtained in Section IV E. For a-SiO2, the propagating, diffuson, and total thermal conductivities are 0.09, 1.92, and 2.01 W/m-K. The total value agrees with the GK value within the errors. Baldi et al. estimated 0.1 W/m-K for the propagating component,[17] while Love and Anderson estimate 0.03 W/m-K.[31] Shenogin et al. predicted the total thermal conductivity of a-SiO2 using non-equilibrium MD simulations of the same small structures used in this work, where 2.0 W/m-K was predicted for the largest system (972 atoms), in good agreement with the total bulk value predicted in this work.[106] We consider the propagating contribution predicted in this work to be an upper-bound considering the lack of defini-

tive scaling of the diffusivities (Fig 5 and the strong non-linear dispersion Fig. 3.(footnote) Within the errors of the predictions, k_{pr} is not a significant fraction of k_{vib} for a-SiO2.

(footnote) The transverse sound speed predicted for our model of a-SiO2 is about 85% of that predicted by the other methods used in the present study and that measured by experiment.[11] While using a smaller transverse sound speed leads to an underprediction of the mode diffusivity scaling (Eq. (4), Fig. 5), it leads to an overprediction of the DOS (Eq. (3)). Holding all other input parameters in Eq. (1) constant, a smaller sound speed leads to a larger k_{pr} because the DOS scales as $DOS(\omega) \propto 1/v_s^3$. In this sense we can regard the prediction for k_{pr} from our model of a-SiO2 as an upper bound. Our model confirms that propagating modes do not contribute significantly to the thermal conductivity of a-SiO2. (footnote)

Assuming an ω^{-2} diffusivity scaling for a-Si the propagating, diffuson, and total thermal conductivity are 0.63, 1.16, and 1.79 W/m-K. This value for total thermal conductivty is in agreement with the GK-predicted bulk value within the errors. At 300 K for a-Si modeled by the Tersoff potential, $k_{ph} \approx k_{AF}$.[55] Earlier studies using similar models of a-Si to those used in this work find that k_{pr} is less than half of k_{vib}.[8,10] Estimates based on experimental measurements have shown k_{pr} as low as 20%[9,10] and as high as 80% k_{vib}.[11,12]

If an ω^{-4} scaling is assumed the resulting diverging conductivity at low frequency is fixed by using a boundary scattering model based on the Matthiessen rule and the thin-film thickness t_f,[107]

$$\frac{1}{\Lambda_{eff}} = \frac{1}{\Lambda_{bulk}} + \frac{2}{t_f}. \tag{25}$$

Using the largest film thickness from the experimental literature(80 μm)(cite) gives a propagating contribution to thermal conductivity of 2.98 W/m-K, much larger than the GK-predicted bulk conductivity. Using the ω^{-2} scaling and this film thickness gives a propagating contribution of 0.63 W/m-K. While predictions for k_{pr} for a-Si depend on the experimental sample preparations[7,9,11,12] and the assumed scaling of the low-frequency vibrational diffusivities[8–12] all evidence supports that k_{pr} is a significant fraction of k_{vib}.[7–12,55]

In Section II A we approximated the specific heat of the propagating and non-propagating (diffusons) modes by the classical-limit value $C(\omega) = k_B$. The full quantum expression for

the specific heat is

$$C(\omega) = k_{\mathrm{B}} \left[\frac{\hbar\omega/2k_{\mathrm{B}}T}{sinh(\hbar\omega/2k_{\mathrm{B}}T)} \right]^2, \tag{26}$$

where T is the temperature and $C(\omega) \approx k_{\mathrm{B}}$ as ω/T goes to zero (classical limit).[8] For a temperature $T = 300$ K, $C(1.52\times10^{13}$ rads/s$) = 0.98k_B$, which is the largest ω_{cut} used for a-SiO2 or a-Si in this work. Using the classical limit for specific heat is a good approximation for the modes considered in k_{pr}, while it is an approximation for the high-frequency modes in our models. For a-SiO2(a-Si), the maximum frequency in the model is $\omega_{max} = 2.48(1.22) \times 10^{14}$ rads/s and $C(\omega) = 0.073(0.47)k_B$. Thus the quantum effect on $C(\omega)$ affects the contribution k_{AF} only, which we can consider to be an temperature-dependent constant in k_{vib}. Using Eq. (26) gives $k_{AF} = 1.44(1.00)$ W/m-K for a-SiO2(a-Si). This correction brings the overestimate of k_{vib} for a-SiO2 into good agreement with experimental measurements.[7,14,15,30] For a-Si the modified k_{AF} is closer to the classical-limit value, which does not significantly change the predicted k_{vib}. Because the change in k_{AF} due to quantum effects are reasonably small for a-Si, we keep the classical-limit value. This allows us to verify that the ω^{-2} scaling (Eq. (7) with $n = 2$) describes the low-frequency contribution k_{pr} for our model of bulk a-Si.

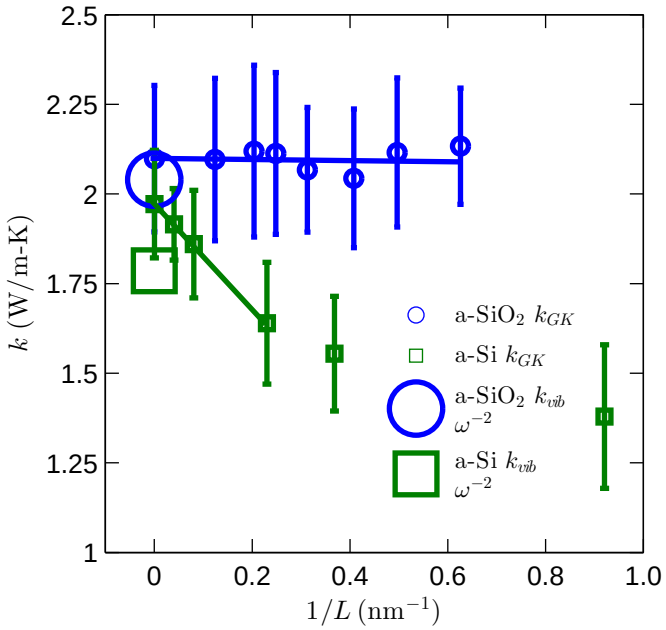

FIG. 6: Thermal conductivities of a-SiO_2 and a-Si predicted using the GK method and Eq. (1). For a-SiO2, the GK-predicted thermal conductivity is size-independent, indicating there is no important contribution from propagating modes. For a-Si, there is a clear size dependance, which is accounted for by predicting the total thermal conductivity [Eq. (1)] with a propagating contribution [Eq. (2)] using an ω^{-2} scaling [Eq. (7)].

B. Accumulation Function

The broadband frequency domain thermal-reflectance measurments by Regner et al.,[7] following the suggestion of Koh and Cahill,[4] interpret the measured thermal conductivity at a given penetration depth to be representative of the so-called thermal conductivity accumulation function. Their results are plotted in Fig. 8 for a 1000 nm thick film of a-SiO2 and in Fig. 7 for 500 nm (Regner A) and 2000 nm (Regner B) thick films for a-Si.[7] Based on the results in Section IV E, we will build thermal conductivity accumulation functions for a-SiO2 and a-Si from

$$k(\Lambda_{max}) = \frac{1}{V}\int_{\Lambda_{max}}^{\Lambda_{cut}} C(\Lambda)D(\Lambda)DOS(\Lambda) + k_{AF}, \tag{27}$$

, where Λ_{cut} is the MFP at the cut-off frequency, Λ_{max} is the maximum MFP considered in the thermal conductivity accumulation, and the MFPs are caculated using Eq. (6). The diffuson contribution k_{AF} is considered a constant (see Section V A. The results are plotted in Figs. 8 and 7.

The predicted thermal conductivity accumulation function for a-SiO2 saturates at a MFP of 10 nm, which is on the order of the finite size of our model. The predicted accumulation for a-SiO2 is demonstrates that propagating contribution is negligible (Section V A). This result is in accord with the penetration depth-independent thermal conductivity measurements using broadband FDTR[7] and experimental measurements which show no film thickness dependance.[14,15] While experiments show there is a cross-over region for the low-frequency diffusivity scaling of ω^{-2} and ω^{-4},[16,20] the propagating contribution was is still shown to be negligible.[31] The cross-over region from ω^{-2} and ω^{-4} scaling observed in experiments for a-SiO2 occurs in the frequency range 4.610^9 to 1.5210^{10} rads/s,[16] and 3.0410^11 to 1.5210^{12} rads/s[20]. Our present model is not large enough to investigate the cross-over region for $n = 2$ to $n = 4$ scaling. The required model size will most likely keep the required frequency range inaccessible for some time to come.

For a-Si, the plateau of thermal conductivity in the measurements of Regner is consistent with our prediction of k_{AF}. For a-Si, the propagating contribution is predicted using both ω^{-2} and ω^{-4} scalings. As discussed in Section V, the ω^{-2} scaling best describes the propagating contribution for our model of bulk a-Si. The thermal conductivity accumulation for the ω^{-2} scaling passes reasonably well through the largest penetration depth measurements of Regner, as well as some of the experimental measurements for varying film thicknesses.

The predicted k_{vib} for varying film thickness follows roughly the accumulation function, so the experimentally-measured thermal conductivities are compared directly in Figs. 8 and 7. The experimental measurements are grouped broadly by sample preparation technique: (A) chemical vapor deposition[11,12,26] and (B) sputtered.[9,24,25]

We consider the ω^{-4} scaling with the boundary scattering model [Eq. (25)] and an 80,000 nm thick film. The measurements of Regner show much sharper accumulations than either ω^{-2} or ω^{-4} scalings, particularly for a film of thickness 2000 nm. Because of the large variation in experimental measurements, predictions for both ω^{-2} and ω^{-4} pass reasonably well through the experimental measurments of Regner and thin films. Amorphous silicon can be prepared only in thin films,(cite) where voids and other inhomogeneities are unavoidable[108] and can influence the vibrational structure at low frequencies.[11,109] Our models are not large enough to investigate the relevant frequency range ($< 10^{12}$ rads/s) where the scaling transition may occur. It is worth noting again that the results from thin film experiments have been interpreted using both scalings.[8–12]

Experiments show there is a cross-over of the low-frequency diffusivity scaling in a-SiO2 of ω^{-4} to ω^{-2} in the frequency range 4.610^9 to 1.5210^{10} rads/s[16] and 3.0410^11 to 1.5210^{12} rads/s[20]. Our present model is not large enough to investigate this frequency range. A transition between ω^{-4} and ω^{-2} scalings can be achieved using a phenomenological model where a cross-over frequency must be specified by experiment.[19] While this cross-over frequency can be identified experimentally for a-SiO2,[16] experiments are limited for a-Si thin films.

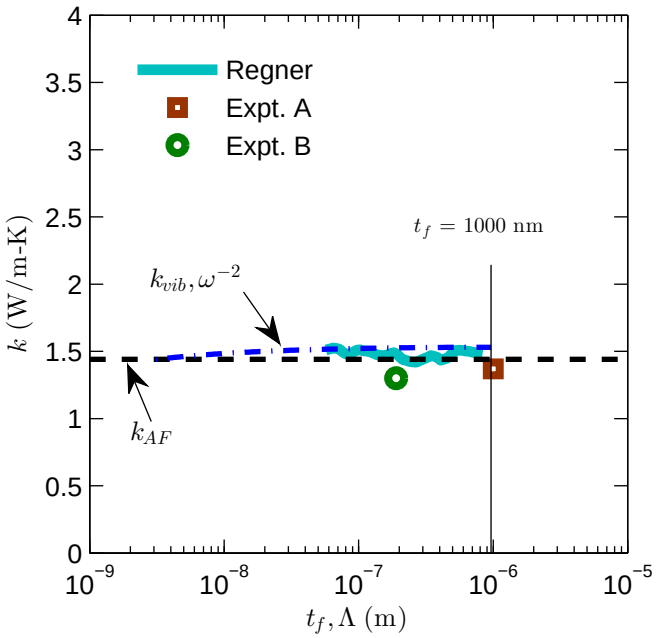

FIG. 7: Predicted thermal conductivity accumulation function [Eq. (27) for a-SiO2 compared with experimental measurements by Regner et al.,[7] Love and Anderson (Expt. A),[31] and Yamane et al. (Expt. B).[15] The predicted thermal conductivity accumulation demonstrates that the propagating contribution is negligible in our model, which is in accord with the experimental measurements.

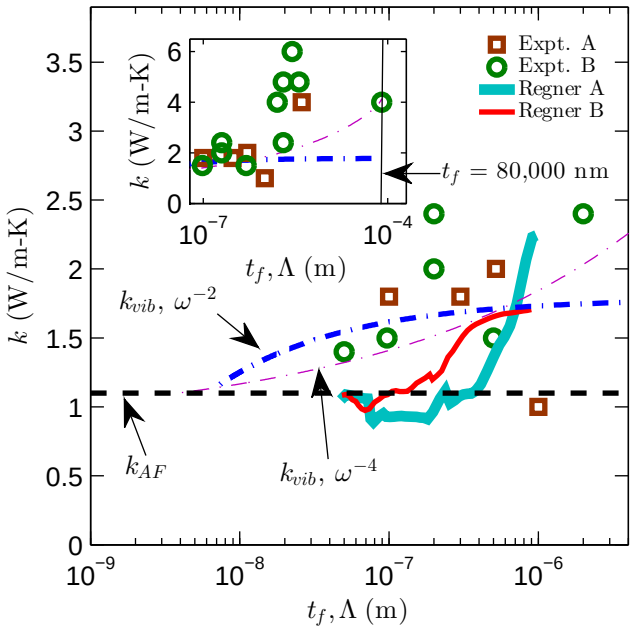

FIG. 8: Predicted thermal conductivity accumulation function [Eq. (27)] for a-Si compared with experimental measurements by Regner et al.[7] and of chemical vapor deposited (Expt. A),[31] and sputtered (Expt. B)[15] thin films with a wide-range of film thicknesses. The predicted thermal conductivity accumulation demonstrates that the propagating contribution is significant for a-Si, while the agreement with the various experimental measurements is only qualititative.

VI. SUMMARY

In this work we investigated the contributions of propagating (k_{ph}) and non-propagating (k_{AF}) modes to the total vibrational thermal conductivity k_{vib} of two amorphous materials, a-SiO2 and a-Si, using the NMD method (Section IV D), GK method (Section V A), and AF theory (Section IV E). Using the NMD method and the AF theory, we predict the total thermal conductivity k_{vib} and its contributions from propagating (k_{pr}) and non-propagating (k_{AF}) using a bottom-up approach based on the mode-by-mode properties. Using the GK method and very-large models (including the largest simulated model of a-Si we are aware of), we predict k_{vib} of bulk a-SiO2 and a-Si. For our model of bulk a-Si the thermal conductivity has significant contribution from propagating modes which are best described by a diffusivity scaling of ω^{-2} (see Section II A). For a-SiO2, the contribution from propagating modes was shown to be negligible (Section V A). The is confirmed by experimental thin film measurements[17,31] and broadband frequency domain thermalreflectance measurements by Regner.[7]

The thermal conductivity accumulation functions predicted for a-Si using both ω^{-2} and ω^{-4} scalings show reasonable agreement with the experimental measurments.[7–12] The large discrepancies between measurments of a-Si thin films suggest that a comprehensive experimental study is necessary on varying film thicknesses and preparation techniques. It may be particularly helpful to perform the broadband techniques[4,5,7] at temperatures less than < 10 K where the propagating contribution dominates for both a-SiO2 and a-Si.[8–12,17,22,29–31]

[1] M. G. Holland, Physical Review **132**, 2461 (1963).

[2] A. D. Christianson, M. D. Lumsden, O. Delaire, M. B. Stone, D. L. Abernathy, M. A. McGuire, A. S. Sefat, R. Jin, B. C. Sales, D. Mandrus, et al., Phys. Rev. Lett. **101**, 157004 (2008), URL http://link.aps.org/doi/10.1103/PhysRevLett.101.157004.

[3] M. Highland, B. C. Gundrum, Y. K. Koh, R. S. Averback, D. G. Cahill, V. C. Elarde, J. J. Coleman, D. A. Walko, and E. C. Landahl, Phys. Rev. B **76**, 075337 (2007), URL http://link.aps.org/doi/10.1103/PhysRevB.76.075337.

[4] Y. K. Koh and D. G. Cahill, Phys. Rev. B **76**, 075207 (2007), URL http://link.aps.org/doi/10.1103/PhysRevB.76.075207.

[5] A. J. Minnich, J. A. Johnson, A. J. Schmidt, K. Esfarjani, M. S. Dresselhaus, K. A. Nelson, and G. Chen, Phys. Rev. Lett. **107**, 095901 (2011), URL http://link.aps.org/doi/10.1103/PhysRevLett.107.095901.

[6] F. Yang and C. Dames, Physical Review B **87**, 035437 (2013), URL http://link.aps.org/doi/10.1103/PhysRevB.87.035437.

[7] K. T. Regner, D. P. Sellan, Z. Su, C. H. Amon, A. J. McGaughey, and J. A. Malen, Nat Commun **4**, 1640 (2013), URL http://dx.doi.org/10.1038/ncomms2630.

[8] J. L. Feldman, M. D. Kluge, P. B. Allen, and F. Wooten, Physical Review B **48**, 1258912602 (1993).

[9] D. G. Cahill, M. Katiyar, and J. R. Abelson, Physical Review B **50**, 60776081 (1994).

[10] J. L. Feldman, P. B. Allen, and S. R. Bickham, Phys. Rev. B **59**, 35513559 (1999), URL http://link.aps.org/doi/10.1103/PhysRevB.59.3551.

[11] X. Liu, J. L. Feldman, D. G. Cahill, R. S. Crandall, N. Bernstein, D. M. Photiadis, M. J. Mehl, and D. A. Papaconstantopoulos, Phys. Rev. Lett. **102**, 035901 (2009), URL http://link.aps.org/doi/10.1103/PhysRevLett.102.035901.

[12] H.-S. Yang, D. G. Cahill, X. Liu, J. L. Feldman, R. S. Crandall, B. A. Sperling, and J. R. Abelson, Phys. Rev. B **81**, 104203 (2010), URL http://link.aps.org/doi/10.1103/PhysRevB.81.104203.

[13] Y. He, D. Donadio, J.-H. Lee, J. C. Grossman, and G. Galli, ACS Nano **5**, 1839\textbackslashtextbackslashtextbackslashtextbackslashtextbackslash961844 (2011).

[14] S.-M. Lee and D. G. Cahill, Journal of Applied Physics **81**, 25902595 (1997).

[15] T. Yamane, N. Nagai, S.-i. Katayama, and M. Todoki, Journal of Applied Physics **91**, 97729776 (2002), URL http://link.aip.org/link/?JAP/91/9772/1.

[16] C. Masciovecchio, G. Baldi, S. Caponi, L. Comez, S. Di Fonzo, D. Fioretto, A. Fontana, A. Gessini, S. C. Santucci, F. Sette, et al., Phys. Rev. Lett. **97**, 035501 (2006), URL http://link.aps.org/doi/10.1103/PhysRevLett.97.035501.

[17] G. Baldi, V. M. Giordano, G. Monaco, F. Sette, E. Fabiani, A. Fontana, and G. Ruocco, Phys. Rev. B **77**, 214309 (2008), URL http://link.aps.org/doi/10.1103/PhysRevB.77.214309.

[18] G. Baldi, V. M. Giordano, G. Monaco, and B. Ruta, Phys. Rev. Lett. **104**, 195501 (2010), URL http://link.aps.org/doi/10.1103/PhysRevLett.104.195501.

[19] G. Baldi, V. M. Giordano, and G. Monaco, Phys. Rev. B **83**, 174203 (2011), URL http://link.aps.org/doi/10.1103/PhysRevB.83.174203.

[20] G. Baldi, M. Zanatta, E. Gilioli, V. Milman, K. Refson, B. Wehinger, B. Winkler, A. Fontana, and G. Monaco, Phys. Rev. Lett. **110**, 185503 (2013), URL http://link.aps.org/doi/10.1103/PhysRevLett.110.185503.

[21] G. Pompe and E. Hegenbarth, physica status solidi (b) **147**, 103 (1988), ISSN 1521-3951, URL http://dx.doi.org/10.1002/pssb.2221470109.

[22] D. G. Cahill, H. E. Fischer, T. Klitsner, E. T. Swartz, and R. O. Pohl, Journal of Vaccuum Science and Technology A **7**, 12591266 (1989).

[23] L. Wieczorek, H. Goldsmid, and G. Paul, in *Thermal Conductivity 20*, edited by D. Hasselman and J. Thomas, J.R. (Springer US, 1989), pp. 235–241, ISBN 978-1-4612-8069-9, URL http://dx.doi.org/10.1007/978-1-4613-0761-7_22.

[24] B. S. W. Kuo, J. C. M. Li, and A. W. Schmid, Applied Physics A: Materials Science & Processing **55**, 289296 (1992), ISSN 0947-8396, 10.1007/BF00348399, URL http://dx.doi.org/10.1007/BF00348399.

[25] H. Wada and T. Kamijoh, Japanese Journal of Applied Physics **35**, L648L650 (1996), URL http://jjap.jsap.jp/link?JJAP/35/L648/.

[26] S. Moon, M. Hatano, M. Lee, and C. P. Grigoropoulos, International Journal of Heat and Mass Transfer **45**, 2439 2447 (2002), ISSN 0017-9310, URL http://www.sciencedirect.com/science/article/pii/S0017931001003477.

[27] B. L. Zink, R. Pietri, and F. Hellman, Physical Review Letters **96**, 055902 (2006), URL

http://link.aps.org/doi/10.1103/PhysRevLett.96.055902.

[28] B. L. Zink, R. Islam, D. J. Smith, and F. Hellman, Phys. Rev. B **74**, 205209 (2006), URL http://link.aps.org/doi/10.1103/PhysRevB.74.205209.

[29] J. J. Freeman and A. C. Anderson, Physical Review B **34**, 5684\textbackslashtextbackslashtextbackslash965690 (1986).

[30] D. Cahill and R. Pohl, Annual Review of Physical Chemistry **39**, 93121 (1988).

[31] M. S. Love and A. C. Anderson, Phys. Rev. B **42**, 18451847 (1990), URL http://link.aps.org/doi/10.1103/PhysRevB.42.1845.

[32] N. W. Ashcroft and N. D. Mermin, *Solid State Physics* (Saunders, Fort Worth, 1976).

[33] M. T. Dove, *Introduction to Lattice Dynamics* (Cambridge, Cambridge, 1993).

[34] J. M. Ziman, *Electrons and Phonons* (Oxford, New York, 2001).

[35] D. A. McQuarrie, *Statistical Mechanics* (University Science Books, Sausalito, 2000).

[36] R. Vacher, J. Pelous, F. Plicque, and A. Zarembowitch, Journal of Non-Crystalline Solids **45**, 397 (1981), ISSN 0022-3093, URL http://www.sciencedirect.com/science/article/pii/0022309381900600.

[37] C. J. Morath and H. J. Maris, Phys. Rev. B **54**, 203213 (1996), URL http://link.aps.org/doi/10.1103/PhysRevB.54.203.

[38] P. Benassi, M. Krisch, C. Masciovecchio, V. Mazzacurati, G. Monaco, G. Ruocco, F. Sette, and R. Verbeni, Phys. Rev. Lett. **77**, 38353838 (1996), URL http://link.aps.org/doi/10.1103/PhysRevLett.77.3835.

[39] S. N. Taraskin and S. R. Elliott, Philosophical Magazine Part B **79**, 17471754 (1999), URL http://www.tandfonline.com/doi/abs/10.1080/13642819908223057.

[40] S. N. Taraskin and S. R. Elliott, Phys. Rev. B **61**, 1201712030 (2000), URL http://link.aps.org/doi/10.1103/PhysRevB.61.12017.

[41] W. Gtze and M. R. Mayr, Phys. Rev. E **61**, 587606 (2000), URL http://link.aps.org/doi/10.1103/PhysRevE.61.587.

[42] G. Ruocco, F. Sette, R. Di Leonardo, G. Monaco, M. Sampoli, T. Scopigno, and G. Viliani, Phys. Rev. Lett. **84**, 57885791 (2000), URL http://link.aps.org/doi/10.1103/PhysRevLett.84.5788.

[43] G. Ruocco and F. Sette, Journal of Physics: Condensed Matter **13**, 9141 (2001), URL http://stacks.iop.org/0953-8984/13/i=41/a=307.

[44] J. Horbach, W. Kob, and K. Binder, The European Physical Journal B - Condensed Matter and Complex Systems **19**, 531 (2001), ISSN 1434-6028, URL http://dx.doi.org/10.1007/s100510170299.

[45] A. Matic, D. Engberg, C. Masciovecchio, and L. Brjesson, Phys. Rev. Lett. **86**, 38033806 (2001), URL http://link.aps.org/doi/10.1103/PhysRevLett.86.3803.

[46] J. L. Feldman, Journal of Non-Crystalline Solids **307310**, 128 (2002), ISSN 0022-3093, URL http://www.sciencedirect.com/science/article/pii/S0022309302014503.

[47] B. Ruffl, M. Foret, E. Courtens, R. Vacher, and G. Monaco, Phys. Rev. Lett. **90**, 095502 (2003), URL http://link.aps.org/doi/10.1103/PhysRevLett.90.095502.

[48] W. Schirmacher, G. Ruocco, and T. Scopigno, Phys. Rev. Lett. **98**, 025501 (2007), URL http://link.aps.org/doi/10.1103/PhysRevLett.98.025501.

[49] J. K. Christie, S. N. Taraskin, and S. R. Elliott, Journal of Non-Crystalline Solids **353**, 2272 (2007), ISSN 0022-3093, URL http://www.sciencedirect.com/science/article/pii/S0022309307002840.

[50] H. Shintani and H. Tanaka, Nat Mater **7**, 870 (2008), ISSN 1476-1122, URL http://dx.doi.org/10.1038/nmat2293.

[51] N. Xu, V. Vitelli, M. Wyart, A. J. Liu, and S. R. Nagel, Phys. Rev. Lett. **102**, 038001 (2009), URL http://link.aps.org/doi/10.1103/PhysRevLett.102.038001.

[52] C. Ganter and W. Schirmacher, Phys. Rev. B **82**, 094205 (2010), URL http://link.aps.org/doi/10.1103/PhysRevB.82.094205.

[53] V. Vitelli, N. Xu, M. Wyart, A. J. Liu, and S. R. Nagel, Phys. Rev. E **81**, 021301 (2010), URL http://link.aps.org/doi/10.1103/PhysRevE.81.021301.

[54] M. Wyart, EPL (Europhysics Letters) **89**, 64001 (2010), URL http://stacks.iop.org/0295-5075/89/i=6/a=64001.

[55] Y. He, D. Donadio, and G. Galli, Applied Physics Letters **98**, 144101 (2011), URL http://link.aip.org/link/?APL/98/144101/1.

[56] S. Ayrinhac, M. Foret, A. Devos, B. Ruffl, E. Courtens, and R. Vacher, Phys. Rev. B **83**, 014204 (2011), URL http://link.aps.org/doi/10.1103/PhysRevB.83.014204.

[57] J. Callaway, Physical Review **113**, 1046 (1959).

[58] P. G. Klemens, Proceedings of the Physical Society. Section A **68** (1955).

[59] P. B. Allen and J. L. Feldman, Physical Review B **48**, 1258112588 (1993).

[60] C. Kittel, Physical Review **75**, 974 (1949).

[61] R. O. Pohl, X. Liu, and E. Thompson, Rev. Mod. Phys. **74**, 9911013 (2002), URL http://link.aps.org/doi/10.1103/RevModPhys.74.991.

[62] G. C. Sosso, D. Donadio, S. Caravati, J. Behler, and M. Bernasconi, Phys. Rev. B **86**, 104301 (2012), URL http://link.aps.org/doi/10.1103/PhysRevB.86.104301.

[63] J. Larkin and A. McGaughey, Journal of Applied Physics (2013).

[64] J. E. Graebner, B. Golding, and L. C. Allen, Phys. Rev. B **34**, 56965701 (1986), URL http://link.aps.org/doi/10.1103/PhysRevB.34.5696.

[65] A. J. H. McGaughey and M. Kaviany, International Journal of Heat and Mass Transfer **47**, 17831798 (2004).

[66] D. Wolf, P. Keblinski, S. R. Phillpot, and J. Eggebrecht, The Journal of Chemical Physics **110**, 8254 (1999), URL http://link.aip.org/link/?JCP/110/8254/1.

[67] G. T. Barkema and N. Mousseau, Phys. Rev. B **62**, 49854990 (2000), URL http://link.aps.org/doi/10.1103/PhysRevB.62.4985.

[68] F. H. Stillinger and T. A. Weber, Physical Review B **31**, 52625271 (1985).

[69] M. Durandurdu and D. A. Drabold, Phys. Rev. B **66**, 155205 (2002), URL http://link.aps.org/doi/10.1103/PhysRevB.66.155205.

[70] N. Bernstein, J. L. Feldman, and M. Fornari, Phys. Rev. B **74**, 205202 (2006), URL http://link.aps.org/doi/10.1103/PhysRevB.74.205202.

[71] K. Momma and F. Izumi, Journal of Applied Crystallography **41**, 653658 (2008), URL http://dx.doi.org/10.1107/S0021889808012016.

[72] S. Plimpton, Journal of Computational Physics **117**, 1 19 (1995), ISSN 0021-9991, URL http://www.sciencedirect.com/science/article/pii/S002199918571039X.

[73] J. Chen, G. Zhang, and B. Li, Physics Letters A **374**, 23922396 (2010), ISSN 0375-9601, URL http://www.sciencedirect.com/science/article/pii/S0375960110004081.

[74] J. D. Gale and A. L. Rohl, Molecular Simulation **29**, 291 (2003).

[75] M. L. Williams and H. J. Maris, Phys. Rev. B **31**, 45084515 (1985), URL http://link.aps.org/doi/10.1103/PhysRevB.31.4508.

[76] D. Donadio and G. Galli, Phys. Rev. Lett. **102**, 195901 (2009).

[77] D. Kaya, N. L. Green, C. E. Maloney, and M. F. Islam, Science **329**, 656 (2010), URL http://www.sciencemag.org/content/329/5992/656.abstract.

[78] N. L. Green, D. Kaya, C. E. Maloney, and M. F. Islam, Physical Review E **83**, 051404 (2011), URL http://link.aps.org/doi/10.1103/PhysRevE.83.051404.

[79] R. Biswas, A. M. Bouchard, W. A. Kamitakahara, G. S. Grest, and C. M. Soukoulis, Phys. Rev. Lett. **60**, 22802283 (1988), URL http://link.aps.org/doi/10.1103/PhysRevLett.60.2280.

[80] P. B. Allen, J. L. Feldman, J. Fabian, and F. Wooten, Philosophical Magazine B **79**, 17151731 (1999).

[81] S. Volz and G. Chen, Physical Review B **61**, 26512656 (2000).

[82] V. Martin-Mayor, M. Mezard, G. Parisi, and P. Verrocchio, The Journal of Chemical Physics **114**, 8068 (2001), URL http://link.aip.org/link/?JCP/114/8068/1.

[83] S. Ciliberti, T. S. Grigera, V. Martin-Mayor, G. Parisi, and P. Verrocchio, The Journal of Chemical Physics **119**, 8577 (2003), URL http://link.aip.org/link/?JCP/119/8577/1.

[84] Y. M. Beltukov, V. I. Kozub, and D. A. Parshin, Phys. Rev. B **87**, 134203 (2013), URL http://link.aps.org/doi/10.1103/PhysRevB.87.134203.

[85] A. Marruzzo, W. Schirmacher, A. Fratalocchi, and G. Ruocco, Sci. Rep. **3** (2013), URL http://dx.doi.org/10.1038/srep01407.

[86] B. Ruzicka, T. Scopigno, S. Caponi, A. Fontana, O. Pilla, P. Giura, G. Monaco, E. Pontecorvo, G. Ruocco, and F. Sette, Phys. Rev. B **69**, 100201 (2004), URL http://link.aps.org/doi/10.1103/PhysRevB.69.100201.

[87] L. E. Silbert, A. J. Liu, and S. R. Nagel, Phys. Rev. E **79**, 021308 (2009), URL http://link.aps.org/doi/10.1103/PhysRevE.79.021308.

[88] J. C. Duda, T. S. English, D. A. Jordan, P. M. Norris, and W. A. Soffa, Journal of Physics: Condensed Matter **23**, 205401 (2011), URL http://stacks.iop.org/0953-8984/23/i=20/a=205401.

[89] T. Hori, T. Shiga, and J. Shiomi, Journal of Applied Physics **113**, 203514 (2013), URL http://link.aip.org/link/?JAP/113/203514/1.

[90] S. N. Taraskin and S. R. Elliott, EPL (Europhysics Letters) **39**, 37 (1997), URL http://stacks.iop.org/0295-5075/39/i=1/a=037.

[91] A. J. C. Ladd, B. Moran, and W. G. Hoover, Physical Review B **34**, 50585064 (1986).

[92] A. J. H. McGaughey and M. Kaviany, Physical Review B **69**, 094303 (2004).

[93] A. S. Henry and G. Chen, Journal of Computational and Theoretical Nanoscience **5**, 112 (2008).

[94] J. E. Turney, E. S. Landry, A. J. H. McGaughey, and C. H. Amon, Phys. Rev. B **79**, 064301 (2009), URL http://link.aps.org/doi/10.1103/PhysRevB.79.064301.

[95] J. M. Larkin, J. E. Turney, A. D. Massicotte, C. H. Amon, and A. J. H. McGaughey, to appear in Journal of Computational and Theoretical Nanoscience (2012).

[96] Y. He, D. Donadio, and G. Galli, Nano Letters **11**, 3608\textbackslashtextbackslashtextbackslashtextbackslash963611 (2011).

[97] Y. He, I. Savic, D. Donadio, and G. Galli, Phys. Chem. Chem. Phys. p. (2012), URL http://dx.doi.org/10.1039/C2CP42394D.

[98] P. Sheng and M. Zhou, Science **253**, 539542 (1991), URL http://www.sciencemag.org/content/253/5019/539.abstract.

[99] V. Mazzacurati, G. Ruocco, and M. Sampoli, EPL (Europhysics Letters) **34**, 681 (1996), URL http://stacks.iop.org/0295-5075/34/i=9/a=681.

[100] S. R. Bickham and J. L. Feldman, Phys. Rev. B **57**, 1223412238 (1998), URL http://link.aps.org/doi/10.1103/PhysRevB.57.12234.

[101] J. Fabian and P. B. Allen, Phys. Rev. Lett. **77**, 38393842 (1996), URL http://link.aps.org/doi/10.1103/PhysRevLett.77.3839.

[102] S. R. Bickham, Phys. Rev. B **59**, 48944897 (1999), URL http://link.aps.org/doi/10.1103/PhysRevB.59.4894.

[103] J. Fabian, J. L. Feldman, C. S. Hellberg, and S. M. Nakhmanson, Phys. Rev. B **67**, 224302 (2003), URL http://link.aps.org/doi/10.1103/PhysRevB.67.224302.

[104] J. Shiomi, K. Esfarjani, and G. Chen, Physical Review B **84**, 125209 (2011).

[105] K. Esfarjani, G. Chen, and H. T. Stokes, Physical Review B **84**, 085204 (2011).

[106] S. Shenogin, A. Bodapati, P. Keblinski, and A. J. H. McGaughey, Journal of Applied Physics **105**, 034906 (2009), URL http://link.aip.org/link/?JAP/105/034906/1.

[107] D. P. Sellan, J. E. Turney, A. J. H. McGaughey, and C. H. Amon, Journal of Applied Physics **108**, 113524 (2010).

[108] S. Li, Y. Jiang, Z. Wu, J. Wu, Z. Ying, Z. Wang, W. Li, and G. J. Salamo, Applied Surface Science **257**, 8326 (2011), ISSN 0169-4332, URL http://www.sciencedirect.com/science/article/pii/S0169433211004715.

[109] J. L. Feldman, N. Bernstein, D. A. Papaconstantopoulos, and M. J. Mehl, Phys. Rev. B **70**, 165201 (2004), URL http://link.aps.org/doi/10.1103/PhysRevB.70.165201.